

Article

Analysis of a Transversely Isotropic Annular Circular Cylinder Immersed in a Magnetic Field Using the Moore–Gibson–Thompson Thermoelastic Model and Generalized Ohm’s Law

Osama Moaaz ^{1,*}, Ahmed E. Abouelregal ^{2,3,*}  and Fahad Alsharari ² 

¹ Department of Mathematics, College of Science, Qassim University, P.O. Box 6644, Buraydah 51482, Saudi Arabia

² Department of Mathematics, College of Science and Arts, Jouf University, Al-Qurayat 77455, Saudi Arabia

³ Department of Mathematics, Faculty of Science, Mansoura University, Mansoura 35516, Egypt

* Correspondence: o.refaei@qu.edu.sa (O.M.); ahabogal@ju.edu.sa (A.E.A.)

Abstract: The main objective of this work is to study the homogeneous thermoelastic interactions in an isotropic hollow thin cylinder immersed in an electric–magnetic field using the linear Moore–Gibson–Thompson theory of thermoelasticity, taking into account the generalized Ohm’s law. The MGT system of thermoelastic equations for the new model is created by incorporating a relaxation period in the Green–Naghdi type III framework. In addition, the Maxwell equations that investigate the effect of the electromagnetic field are presented. While the outer surface of the hollow cylinder is thermally insulated and free of traction, the interior surface is both free of traction and subject to thermal shock. To convert the problem to the space domain only, the Laplace transform methodology is used to solve the governing equations generated in the transformed domain. The theoretical results are computed dynamically and are graphically displayed for a transversely isotropic material using the Honig and Hirdes approach. A comparison of findings based on different (classical and generalized) thermoelastic theories is provided, followed by a discussion on the impact of the applied electromagnetic field.

Keywords: thermoelasticity; generalized Ohm’s law; transverse hollow cylinder; magneto-electro-thermo-elastic; MGT equation

MSC: 35B40; 35Q79; 35J55; 45F15; 73B30



Citation: Moaaz, O.; Abouelregal, A.E.; Alsharari, F. Analysis of a Transversely Isotropic Annular Circular Cylinder Immersed in a Magnetic Field Using the Moore–Gibson–Thompson Thermoelastic Model and Generalized Ohm’s Law. *Mathematics* **2022**, *10*, 3816. <https://doi.org/10.3390/math10203816>

Academic Editors: Carlos Llopis-Albert, Yang Liu and Yury Shestopalov

Received: 3 August 2022

Accepted: 9 October 2022

Published: 16 October 2022

Publisher’s Note: MDPI stays neutral with regard to jurisdictional claims in published maps and institutional affiliations.



Copyright: © 2022 by the authors. Licensee MDPI, Basel, Switzerland. This article is an open access article distributed under the terms and conditions of the Creative Commons Attribution (CC BY) license (<https://creativecommons.org/licenses/by/4.0/>).

1. Introduction

The thermomechanical properties of materials vary with temperature. In many structural applications, the structural elements of materials are usually subjected to such extreme temperature changes that even in approximation mode, their material properties cannot be considered to be of constant values. Therefore, the dependence of physical properties on temperature should be taken into consideration during the heat stress analysis of these components. In recent decades, isotropic thermal stress issues have become increasingly significant for modern designs, such as nuclear reactors. This is due to the increased diversity of engineering structures and the prevalence of work in extremely hot environments.

The concept of thermoelasticity describes the effects of mechanical and thermal disturbances on elastic as well as viscous materials. Two equations govern the thermal conductivity theory: one dealing with heat transfer and conduction and the other dealing with motion. For this concept, in the traditional theory, there are two drawbacks. First, the formulation of heat transfer in this concept does not include elastic components. Another

problem is that according to the parabolic heat equation, the temperature can spread at an infinite rate, a claim that experimental data have demonstrated.

In conventional thermoelasticity, stress, tension, or deformations caused by measurable thermal stress are predicted. Generalized thermoelastic models were presented because the use of the concept of traditional thermoelasticity leads to the spread of thermal signals at an infinite rate. In recent years, thermoelasticity has been utilized to calculate stress fields based on low-temperature conditions, which cause their rapid changes through a good signal-to-noise ratio in infrared thermography, but it is only relevant to periodic loads. Based on the concepts of irreversible processes in thermodynamics, Biot [1] developed a theory known as classical thermoelasticity. Hyperbolic motion and parabolic heat transfer equations are used in this framework. Even with the parabolic type of heat conduction equation, it still has an uncorrelated theoretical error. There are modified thermoelastic models in which the mathematical heat transfer model is hyperbolic to remove this drawback of the conventional thermoelastic concept.

To fix the Fourier law of thermal conductivity, Cattaneo [2] introduced one parameter that plays the role of relaxation time. Then, the wave-type equation was formulated in place of the traditional Fourier law. The first modification is attributed to Lord and Shulman [3]. They developed a wave-type heat transfer equation by positing a new law of conduction of heat to repair the conventional Fourier law. The heat flow vector and its time derivative are included in this proposed law. It also has a new parameter that acts as a relaxation period. Since the heat equation in this theory is of the wave type, it ensures that heat and elastic waves propagate at limited velocities. This theory has the same equations of motion and constitutive relationships as both coupled and uncoupled theories. The second extension of the thermocoupled theory is what is referred to as the two-time relaxation thermoelastic model or the rate-dependent thermal conductivity model. Green and Lindsay came up with this second concept [4]. In this case, the thermal conductivity and kinetic equations change, because these two constants, which act as relaxation times and are part of this theory, are present.

Green and Naghdi [5–7] discussed linear and nonlinear models of thermoelastic bodies with and without energy squandering. They suggested three new heat conduction models based on the equivalence of entropy. Their thermoelastic models are known as the GN-I, GN-II, and GN-III models. In a linear system, type I may become the conventional heat equation, while type II and III models predict the limited rate of thermal waves upon linearization. Recent attempts to modify the conventional Fourier formula were conducted by Abouelregal [8–14] by utilizing higher-order time derivatives.

A discrepancy is observed (e.g., in [2–4]) when the conventional Fourier law is applied to wave propagation, which leads to the problem of infinite signal velocity. As a result, many different constitutive relationships for heat flow are considered while formulating the linear and nonlinear sound wave equations and the heat equation. Quintanilla [15] created a novel thermoelastic heat conduction model based on the equation of Moore–Gibson–Thompson [15,16]. Quintanilla [15] suggested a new, improved heat equation that includes a relaxation parameter in the Green–Naghdi theory of type III. The Moore–Gibson–Thompson equation is a third-order-in-time wave equation that describes the nonlinear dispersion of sound and eliminates the unlimited signal velocity conundrum of conventional second-order-in-time heavily damped theories of linear acoustics, which include the Westervelt and Kuznetsov formula. The Moore–Gibson–Thompson (MGT) equation is based on simulations of sound waves with high amplitudes. There are a lot of studies on this subject because it has so many uses, such as using high-intensity ultrasound in medicine and industry for extracorporeal shock waves, light therapy, ultrasonic cleaning, etc. Since the advent of the Moore–Gibson–Thompson equation, many studies on this concept have been performed [17–20]. In recent years, the analysis of thermomechanical and structural interactions among many frameworks has been effectively used [21–26].

In recent years, research and development efforts have heavily focused on creating linear Fresnel reflecting concentrators to transform solar energy into usable forms such as heat and light. Sheikholeslami and Ebrahimpour [27] used multi-way twisted tape (MWTT) to improve the thermal processing of the linear Fresnel reflector (LFR) unit. Singh et al. [28] analyzed the thermal efficiency of a linear Fresnel reflecting solar device with four identical trapezoidal cavity absorbers. Sheikholeslami [29] attached horseshoe-shaped fins to the tube's base, and he put perforated tape through the pipe's middle, all in an effort to increase output. The enhanced thermal characteristics of the working fluid also contributed to the enhanced mixing rate brought about by the usage of dispersed hybrid nano-powders. In addition, he examined how nanoparticles in a honeycomb arrangement affected the melting process of paraffin [30].

Researchers have been studying the phenomena of thermomechanical and electromagnetic interactions among materials since the nineteenth century. Hydrophones were the first devices to use piezoelectric materials around the middle of the 20th century. Before the 1960s, researchers studied the thermomagnetic elasticity theory [31]. There are many applications for this important phenomenon, such as in geophysics, to analyze the behavior of the Earth's magnetic field with respect to seismic waves and damp sound waves within a magnetic field. Studying how thermomechanical and electromagnetic materials interact has also uses in nuclear devices (e.g., in the making of very sensitive magnetometers), electrical power engineering, optics, etc. [32].

The idea of electromagnetic composite structures has only recently emerged in the last two decades. Unlike the monolithic constituent materials, such composites can show field coupling. Ultrasound imaging technologies, sensor systems, electronic controls, transducers, and other developing components can benefit from so-called "smart" materials and composites. It is common to find these materials in various applications [33]. High-tech fields such as lasers, supersonic devices, microwaves, and infrared applications utilize these materials because of their versatility in converting energy types (between mechanical and electromagnetic energies). On the other hand, in magneto-electro-elastic materials, mechanical forces, electric currents, and magnetic fields act similarly [34].

The main objective of presenting this paper is to address the issue of thermoelastic-magnetic interactions that occur in a transversely isotropic circular cylinder within the framework of a new mathematical model of generalized thermoelasticity (MGTTE), which includes the Moore-Gibson-Thompson (MGT) equation. Since the traditional models show that the speed at which the heat wave travels is infinite, the new generalized thermoelastic models are more realistic and better fit the physical observations. Through many studies, these models have proven their effectiveness, especially when trying to deal with theoretical and experimental flow problems involving very short periods of time and high heat, such as those that occur in lasers, power systems, nuclear reactors, etc. In addition, from the results of this work, the equations that govern the behavior of generalized thermoelasticity are derived, taking into consideration the effect of a magnetic field and the generalized Ohm's law.

As an application of the problem, it is postulated that the inner surface of the hollow cylinder has no traction and is subject to a time-dependent thermal shock. In contrast, the outer surface has no traction but is thermally insulated. The problem can be solved using the Laplace transform methodology, while the reflection of the Laplace transform is calculated numerically. Numerical calculations of the physical quantities under study, such as temperature, thermal stresses, and deformations, are collected and compared to theories using graphs and tables. Calculations are made to determine how the non-Fourier effect affects how heat and thermoelastic waves are transmitted under conditions of thermal relaxation and the presence of magnetism. When the current study is compared to previous works, the results are found to be generally compatible.

The following organization forms the general form of the article: In Section 2, the essential equations of Moore-Gibson-Thompson thermoelasticity are stated. In Section 3, the problem statement, including the transversely isotropic annular circular cylinder, is

discussed, while in Section 4, the boundary and initial conditions are introduced. To obtain the problem’s solution in a transformed domain, the Laplace transform approach is applied in Section 5. In Section 6, the Laplace transform is numerically reversed. Section 7 compares the numerical results of the studied fields in three different cases, while Section 8 gives the main conclusions.

2. Basic Equation of Moore–Gibson–Thompson Thermoelastic Model

The constitutive and strain-displacement relations and motion equation for a homogeneous transversely isotropic material are as follows [28–30]:

$$\sigma_{ij} = c_{ijkl}e_{kl} - \beta_{ij}\theta, \tag{1}$$

$$e_{ij} = 0.5(u_{j,i} + u_{i,j}), \tag{2}$$

$$\sigma_{ij,j} + F_i = \rho \frac{\partial^2 u_i}{\partial t^2}. \tag{3}$$

Cattaneo and Vernotte [2,35] developed a generalized form of the Fourier law by including the concept of relaxation time with a heat flow vector differential as follows:

$$\left(1 + \tau_0 \frac{\partial}{\partial t}\right) \vec{q}(\vec{x}, t) = -K \vec{\nabla} \theta(\vec{x}, t). \tag{4}$$

Later on, Green and Naghdi [5–7] created three formulations for extended heat conduction of homogeneous isotropic materials. These concepts are called types I, II, and III, respectively. Using the GN-III model, we can write an improved version of the Fourier law as [6]:

$$\vec{q}(\vec{x}, t) = -\left[K \vec{\nabla} \theta(\vec{x}, t) + K^* \vec{\nabla} \dot{\theta}(\vec{x}, t)\right], \quad \dot{\theta} = \theta. \tag{5}$$

We can see that we can go back to type I (GN-I) when material parameter $K^* = 0$, while type II (GN-II) can be reached at $K = 0$.

The equation for determining the energy balance can be written as [3,4]:

$$\rho C_E \frac{\partial \theta}{\partial t} + T_0 \frac{\partial}{\partial t} (\beta_{ij} e_{ij}) = -q_{i,i} + Q. \tag{6}$$

The modified Fourier law (5) has the same defect as the usual Fourier model in predicting the rapid propagation of heat transfer waves. In this model, the principle of causation is not followed. As a result, this recommendation has been extensively updated, and a relaxation factor has been included to address this issue [15]. Quintanilla [16] formulated the proposed heat equation by adding the relaxation modulus to the Green–Naghdi type III framework. The resulting form of the improved thermal conductivity equation is given by [16,17]:

$$\left(1 + \tau_0 \frac{\partial}{\partial t}\right) \vec{q}(\vec{x}, t) = -\left[K \vec{\nabla} \theta(\vec{x}, t) + K^* \vec{\nabla} \dot{\theta}(\vec{x}, t)\right]. \tag{7}$$

After combining Equations (6) and (7), we have a new linear form of the thermal conductivity equation (MGTTE), which is based on the Moore–Gibson–Thompson equation for an isotropic substance as shown in the following formula:

$$\left(1 + \tau_0 \frac{\partial}{\partial t}\right) \left[\frac{\partial}{\partial t} \left(\rho C_E \frac{\partial \theta}{\partial t}\right) + T_0 \frac{\partial^2}{\partial t^2} (\beta_{ij} e_{ij}) - \frac{\partial Q}{\partial t}\right] = \frac{\partial}{\partial t} [\nabla \cdot (K \nabla \theta)] + \frac{\partial}{\partial t} [\nabla \cdot (K^* \nabla \dot{\theta})]. \tag{8}$$

The latter form is a generalization of both the Lord–Shulman theory (LS) [3] and the third type of the Green–Naghdi theory of thermoelasticity (GN-III) [6].

It is supposed that the surrounding free space has an initial magnetic field \vec{H} that permeates it. To meet the magnetic equations of Maxwell, as well as slow-moving medium, this generates a generated electro-field \vec{E} and a generated magnetic field \vec{h} . Without the displacement current and charge density, the electromagnetic field is described by the following Maxwell equations [36]:

$$\begin{aligned} \vec{J} &= \nabla \times \vec{h} + \frac{\partial \vec{D}}{\partial t}, \quad \nabla \times \vec{E} = -\mu_0 \frac{\partial \vec{B}}{\partial t}, \quad \vec{B} = \mu_0 \vec{H}, \quad \vec{H} = \vec{H}_0 + \vec{h}, \\ \vec{D} &= \epsilon_0 \vec{E}, \quad \nabla \cdot \vec{h} = 0, \quad \nabla \cdot \vec{D} = 0. \end{aligned} \tag{9}$$

The Maxwell stress tensor, τ_{ij} , can be presented by:

$$\tau_{ij} = \mu_0 [H_i h_j + H_j h_i - H_k h_k \delta_{ij}]. \tag{10}$$

When the small effect of temperature gradient on \vec{J} is not taken into account, the generalized form of Ohm’s law for deformable continua can be written as:

$$\vec{J} = \sigma_0 \left[\vec{E} + \frac{\partial \vec{u}}{\partial t} \times \vec{B} \right]. \tag{11}$$

The ability of a material to conduct an electric current is measured only by means of its electrical conductivity. Many materials exhibit varying values of electrical conductivity (σ_0) depending on their ability to allow electricity to pass through. Many researchers take into account that a material is perfectly conductive (zero resistivity); therefore, electrical conductivity would lead to infinity (i.e., $\sigma_0 \rightarrow \infty$). However, this is not physically acceptable, as electrical conductivity, whatever the type of conductive material, is limited. Although there are no perfect electrical conductors in nature, the idea can be used as a model when electrical resistance is insignificant in comparison with other influences.

3. Formulation of the Problem

We consider a thermoelastic body to be an infinitely hollow cylinder made of a homogeneous transversely isotropic material with finite conductivity that has an inner radius a and an outer radius b and is free of traction (see Figure 1). It begins in an undisturbed state at a uniform temperature T_0 when a time-dependent symmetric thermal shock is applied to its inner surface while the outer surface is thermally insulated. We suppose that (r, ξ, z) denote the cylindrical polar coordinates, where the z -axis coincides with the cylinder axis. There are only two variables to consider in this problem: the distance variable, r , and the passage of time, t , due to the cylindrical symmetry of the problem.

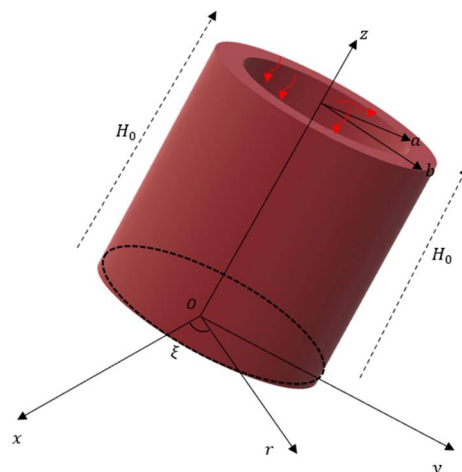


Figure 1. Diagrammatic representation of thermoelastic hollow cylinder.

As a result, the displacement vector involves the following components:

$$\vec{u} = (u_r, u_\zeta, u_z) = (u(r, t), 0, 0). \tag{12}$$

Using this displacement field, the corresponding strain components are derived as:

$$e_{rr} = \frac{\partial u}{\partial r}, \quad e_{\zeta\zeta} = \frac{u}{r}, \quad e_{r\zeta} = e_{zz} = e_{z\zeta} = e_{rz} = 0. \tag{13}$$

Therefore, the cubic dilatation, e , can be expressed as

$$e = e_{rr} + e_{\zeta\zeta} + e_{zz} = \frac{\partial u}{\partial r} + \frac{u}{r} = \frac{1}{r} \frac{\partial}{\partial r}(ru). \tag{14}$$

The components that make up the mechanical stress tensor, σ_{ij} , can be deduced as follows:

$$\begin{bmatrix} \sigma_{rr} \\ \sigma_{\zeta\zeta} \\ \sigma_{zz} \end{bmatrix} = \begin{bmatrix} c_{11} & c_{12} & -\beta_{rr} \\ c_{12} & c_{11} & -\beta_{\zeta\zeta} \\ c_{13} & c_{13} & -\beta_{zz} \end{bmatrix} \begin{bmatrix} \frac{\partial u}{\partial r} \\ \frac{u}{r} \\ \theta \end{bmatrix}, \tag{15}$$

where σ_{rr} , $\sigma_{\zeta\zeta}$, and σ_{zz} represent the normal thermal stresses.

In cylindrical coordinates, the following is the motion equation when external body forces are present:

$$\frac{\partial \sigma_{rr}}{\partial r} + \frac{\sigma_{rr} - \sigma_{\zeta\zeta}}{r} + F_r = \rho \frac{\partial^2 u}{\partial t^2} \tag{16}$$

where F_r represents the Lorentz force due to the presence of the magnetic field, which can be determined from the following relationship:

$$F_r = \left(\vec{J} \times \vec{B} \right)_r. \tag{17}$$

We take into account that the applied initial magnetic field, \vec{H}_0 , and the induced magnetic field, \vec{h} , have the following components:

$$\vec{H}_0 = (0, 0, H_0), \quad \vec{h} = (0, 0, h). \tag{18}$$

These equations clearly show that the non-vanishing components of vectors \vec{J} and \vec{E} only exist in the ζ -direction, i.e.,:

$$\vec{J} = (0, J, 0), \quad \vec{E} = (0, E, 0). \tag{19}$$

A linearization of Ohm’s law (11) yields:

$$J = \sigma_0 \left[E - \mu_0 H_0 \frac{\partial u}{\partial t} \right]. \tag{20}$$

In our situation, we can obtain the following two equations from Equation (9):

$$\begin{aligned} \frac{\partial h}{\partial r} &= - \left[J + \epsilon_0 \frac{\partial E}{\partial t} \right], \\ \frac{1}{r} \frac{\partial}{\partial r}(rE) &= -\mu_0 \frac{\partial h}{\partial t}. \end{aligned} \tag{21}$$

In the free space surrounding the cylinder, we can obtain the following two equations:

$$\begin{aligned} \frac{\partial h^0}{\partial r} &= -\epsilon_0 \frac{\partial E^0}{\partial t}, \\ \frac{1}{r} \frac{\partial}{\partial r}(rE^0) &= -\mu_0 \frac{\partial h^0}{\partial t}, \end{aligned} \tag{22}$$

where E^0 and h^0 denote, respectively, the component of the electric field intensity and the induced magnetic field in free space surrounding the cylinder in the ζ -direction.

By removing variable J from Equations (20) and (21), we arrive at:

$$\frac{\partial h}{\partial r} = \sigma_0 \mu_0 H_0 \frac{\partial u}{\partial t} - \left[\sigma_0 E + \epsilon_0 \frac{\partial E}{\partial t} \right]. \tag{23}$$

Again, when we remove E from Equations (21) and (23), and we obtain:

$$\left[\nabla^2 - \sigma_0 \mu_0 \frac{\partial}{\partial t} - \epsilon_0 \mu_0 \frac{\partial^2}{\partial t^2} \right] h = \sigma_0 \mu_0 H_0 \frac{\partial e}{\partial t}. \tag{24}$$

where $\nabla^2 = \frac{\partial^2}{\partial r^2} + \frac{1}{r} \frac{\partial}{\partial r}$ denotes the Laplace operator.

In our case, the radial component of the Maxwell stress tensor, τ_{ij} , is determined by:

$$\tau_{rr} = -\mu_0 H_0 h. \tag{25}$$

The equation that describes the body force (Lorentz force) in the radial direction is as follows:

$$F_r = \left(\vec{J} \times \vec{B} \right)_r = -\mu_0 H_0 \frac{\partial h}{\partial r}. \tag{26}$$

When Equations (15), (16), and (26), respectively, are used, the motion equation has the form:

$$c_{11} \left(\frac{\partial}{\partial r} + \frac{1}{r} \right) \left(\frac{\partial u}{\partial r} \right) - \beta_{rr} \frac{\partial \theta}{\partial r} - \mu_0 H_0 \frac{\partial h}{\partial r} = (\beta_{rr} - \beta_{\zeta\zeta}) \frac{\theta}{r} + \rho \frac{\partial^2 u}{\partial t^2} \tag{27}$$

Given that $\beta_{rr} = \beta_{\zeta\zeta}$ for a transversely isotropic body, we may derive the following equation by applying the div operator on both sides:

$$c_{11} \nabla^2 e - \beta_{rr} \nabla^2 \theta - \mu_0 H_0 \nabla^2 h = \rho \frac{\partial^2 e}{\partial t^2}. \tag{28}$$

In addition, the modified Moore–Gibson–Thompson heat conduction equation (MGTTE) (8) may be written as:

$$\left(1 + \tau_0 \frac{\partial}{\partial t} \right) \left[\rho C_E \frac{\partial^2 \theta}{\partial t^2} + T_0 \beta_{rr} \frac{\partial^2 e}{\partial t^2} \right] = K \frac{\partial}{\partial t} \nabla^2 \theta + K^* \nabla^2 \theta. \tag{29}$$

The following non-dimensional variables are used to simplify the system equations:

$$\begin{aligned} \{u', r', a', b'\} &= \vartheta \omega \{u, r, a, b\}, & \{t', \tau'_0\} &= \vartheta^2 \omega \{t, \tau_0\}, & \theta' &= \frac{\theta}{T_0}, & \sigma'_{ij} &= \frac{\sigma_{ij}}{c_{11}}, \\ \tau'_{ij} &= \frac{\tau_{ij}}{c_{11}}, & h' &= \frac{\omega \varphi}{\sigma_0 \mu_0 H_0} h, & E' &= \frac{\omega \varphi}{\vartheta \sigma_0 \mu_0^2 H_0} E, & \vartheta^2 &= \frac{c_{11}}{\rho}, & \omega &= \frac{\rho C_E}{K}. \end{aligned} \tag{30}$$

After removing the dashes for simplicity, the governing Equations (22)–(24), (27), and (28) may be reduced to:

$$\frac{\partial h}{\partial r} = \frac{\partial u}{\partial t} - \left[m_0 E + V^2 \frac{\partial E}{\partial t} \right], \tag{31}$$

$$\left[\nabla^2 - m_0 \frac{\partial}{\partial t} - V^2 \frac{\partial^2}{\partial t^2} \right] h = \frac{\partial e}{\partial t}, \tag{32}$$

$$\begin{aligned} \frac{\partial h^0}{\partial r} &= -V^2 \frac{\partial E^0}{\partial t}, \\ \frac{1}{r} \frac{\partial}{\partial r} (r E^0) &= -\frac{\partial h^0}{\partial t}, \end{aligned} \tag{33}$$

$$\nabla^2 e - \delta_1 \nabla^2 \theta - m_0 \delta_2 \nabla^2 h = \frac{\partial^2 e}{\partial t^2}, \tag{34}$$

$$\left(1 + \tau_0 \frac{\partial}{\partial t}\right) \left[\frac{\partial^2 \theta}{\partial t^2} + \delta_1 \frac{\partial^2 e}{\partial t^2}\right] = \frac{\partial}{\partial t} \nabla^2 \theta + \delta_3 \nabla^2 \theta, \tag{35}$$

where:

$$m_0 = \frac{\sigma_0 \mu_0}{\omega}, \quad V = \frac{\vartheta}{c_L}, \quad c_L = \frac{1}{\mu_0 \epsilon_0}, \quad \delta_1 = \frac{T_0 \beta_{rr}}{c_{11}}, \quad \delta_2 = \frac{H_0 \mu_0}{\rho \vartheta^2}, \quad \delta_3 = \frac{K^*}{\vartheta^2 K}. \tag{36}$$

Parameter m_0 is an indicator of magnetic viscosity, while c_L denotes the light speed. If m_0 , V^2 , and δ_2 are all equal to zero, the above formulations simplify the standard generalized thermoelasticity equations without including magneto-electric influences.

In addition, the non-dimensional constitutive equations may be expressed as:

$$\begin{bmatrix} \sigma_{rr} \\ \sigma_{\xi\xi} \\ \sigma_{zz} \end{bmatrix} = \begin{bmatrix} 1 & c_1 & -\delta_1 \\ c_1 & 1 & -\delta_1 \\ c_2 & c_2 & -\delta_4 \end{bmatrix} \begin{bmatrix} \frac{\partial u}{\partial r} \\ u \\ \theta \end{bmatrix}, \tag{37}$$

$$\tau_{rr} = -\delta_2 m_0 h, \tag{38}$$

where:

$$c_1 = \frac{c_{12}}{c_{11}}, \quad c_2 = \frac{c_{13}}{c_{11}}, \quad \delta_4 = \frac{T_0 \beta_{zz}}{c_{11}}. \tag{39}$$

4. Conditions of the Problem

We assume that the conditions for the beginning of the problem are homogeneous during this discussion, i.e.,:

$$u(r, t)|_{t=0} = 0 = \frac{\partial u(r, t)}{\partial t} \Big|_{t=0}, \quad \theta(r, t)|_{t=0} = 0 = \frac{\partial \theta(r, t)}{\partial t} \Big|_{t=0}. \tag{40}$$

We examine infinitely long hollow cylinders with traction-free inner surfaces ($r = a$) that are exposed to a heat shock. As a result, the associated boundary conditions are as follows:

$$\theta(r, t) = \theta_0 H(t) \quad \text{at } r = a, \tag{41}$$

where θ_0 is constant.

The cylinder is considered to have a thermally insulated outer surface, i.e.,:

$$K \frac{\partial \theta(r, t)}{\partial r} = 0 \quad \text{at } r = b. \tag{42}$$

There are no tractions on the interior or external surfaces of the hollow cylinder. Then, we have:

$$\sigma_{rr}(r, t) = 0 \quad \text{at } r = a, \tag{43}$$

$$\sigma_{rr}(r, t) = 0 \quad \text{at } r = b. \tag{44}$$

Vector E has continuous transverse components along the cylinder's inner and outer surfaces, which results in:

$$E(r, t) = E^0(r, t) \quad \text{at } r = a, b. \tag{45}$$

In addition, given that the transverse components of vector h are continuous over the cylinder's inner and outer surfaces, we have:

$$h(r, t) = h^0(r, t) \quad \text{at } r = a, b. \tag{46}$$

5. Problem-Solving Approach Using Laplace Transform

Many areas of practical mathematics benefit significantly from the Laplace transform approach. Functions, measurements, and distributions are just a few of the numerous things that may be used to create it. After transforming Equations (31)–(38), using the Laplace transform under the starting conditions given in Equation (40) leads to:

$$\frac{d\bar{h}}{dr} = s\bar{u} - \varphi_1\bar{E}, \tag{47}$$

$$\begin{aligned} \frac{d\bar{h}^0}{dr} &= -sV^2\bar{E}^0, \\ \frac{1}{r} \frac{d}{dr} (r\bar{E}^0) &= -s\bar{h}^0, \end{aligned} \tag{48}$$

$$\begin{bmatrix} \bar{\sigma}_{rr} \\ \bar{\sigma}_{\xi\xi} \\ \bar{\sigma}_{zz} \end{bmatrix} = \begin{bmatrix} 1 & c_1 & -\delta_1 \\ c_1 & 1 & -\delta_1 \\ c_2 & c_2 & -\delta_4 \end{bmatrix} \begin{bmatrix} \frac{d\bar{u}}{dr} \\ \frac{\bar{u}}{r} \\ \bar{\theta} \end{bmatrix}, \tag{49}$$

$$\bar{\tau}_{rr} = -\delta_2 m_0 \bar{h}, \tag{50}$$

$$(\nabla^2 - s^2)\bar{e} = \delta_1 \nabla^2 \bar{\theta} + m_0 \delta_2 \nabla^2 \bar{h}, \tag{51}$$

$$q\delta_1 \bar{e} = (\nabla^2 - q)\bar{\theta}, \tag{52}$$

$$[\nabla^2 - \varphi_2]\bar{h} = s\bar{e}, \tag{53}$$

where:

$$\varphi_1 = m_0 + sV^2, \quad \varphi_2 = s\varphi_1, \quad q = \frac{s^2(1 + \tau_0 s)}{(s + \delta_3)}. \tag{54}$$

The following sixth-order differential equation is fulfilled by \bar{e} after removing $\bar{\theta}$ and \bar{h} from Equations (51)–(53):

$$(\nabla^6 - A\nabla^4 + B\nabla^2 - C)\bar{e} = 0, \tag{55}$$

where:

$$\begin{aligned} A &= q + \alpha_1 + \frac{\alpha_3}{\alpha_4}, \quad B = \alpha_1 q + \alpha_2 + \frac{\varphi_2 \alpha_3}{\alpha_4}, \quad C = q\alpha_2, \\ \alpha_1 &= s^2 + \varphi_2 + sm_0\delta_2, \quad \alpha_2 = s^2\varphi_2, \quad \alpha_3 = s\delta_1, \quad \alpha_4 = \frac{s}{q\delta_1}. \end{aligned} \tag{56}$$

The factorization of Equation (36) yields:

$$(\nabla^2 - m_1^2)(\nabla^2 - m_2^2)(\nabla^2 - m_3^2)\bar{e} = 0, \tag{57}$$

where $m_1^2, m_2^2,$ and m_3^2 denote the solutions to the following characteristic polynomial:

$$m^6 - Am^4 + Bm^2 - C = 0 \tag{58}$$

The following is a valid representation of the solution to the Bessel Equation (57), which can be expressed as:

$$\bar{e} = \sum_{i=1}^3 [A_i I_0(m_i r) + B_i K_0(m_i r)], \tag{59}$$

where $I_0(m_i r)$ and $K_0(m_i r)$ are the first and second kinds of modified Bessel functions of order zero, and A_i and $B_i,$ with $i = 1, 2, 3,$ are some parameters that depend only on $s.$

We may write the following solutions similarly:

$$\bar{\theta} = \sum_{i=1}^3 [A'_i I_0(m_i r) + B'_i K_0(m_i r)], \tag{60}$$

$$\bar{h} = \sum_{i=1}^3 [A''_i I_0(m_i r) + B''_i K_0(m_i r)]. \tag{61}$$

Equations (52) and (53), which are compatible with these equations, provide:

$$\{A'_i, B'_i\} = \left(\frac{q\delta_1}{m_i^2 - q}\right) \{A_i, B_i\}, \quad \{A''_i, B''_i\} = \left(\frac{s}{m_i^2 - \varphi_2}\right) \{A_i, B_i\}, \quad i = 1, 2, 3. \tag{62}$$

When Equation (59) is substituted into Equation (14), which is integrated concerning r , it yields the following result:

$$\bar{u} = \sum_{i=1}^3 \frac{1}{m_i} [A_i I_1(m_i r) - B_i K_1(m_i r)]. \tag{63}$$

Displacement \bar{u} can be derived using the Bessel function's well-known relations, which are as follows:

$$\begin{aligned} I'_n(x) &= I_{n+1}(x) + \frac{n}{x} K_n(x), & I'_n(x) &= I_{n-1}(x) - \frac{n}{x} K_n(x), \\ K'_n(x) &= -K_{n+1}(x) + \frac{n}{x} K_n(x), & K'_n(x) &= -K_{n-1}(x) - \frac{n}{x} K_n(x). \end{aligned} \tag{64}$$

When we enter the values from Equations (61) and (63) into Equation (47), we obtain:

$$\bar{E} = \sum_{i=1}^3 \frac{-s^2}{m_i(m_i^2 - s\varphi_2)} [A_i I_1(m_i r) - B_i K_1(m_i r)]. \tag{65}$$

The induced fields in free space, \bar{E}^0 and \bar{h}^0 , are obtained by removing \bar{E}^0 between Equation (48) to yield:

$$(\nabla^2 - s^2 V^2) \bar{h}^0 = 0. \tag{66}$$

Equation (49) has a solution that is limited at the origin and at infinity, respectively, and is provided by:

$$\bar{h}^{01} = A_4 I_0(sVr). \tag{67}$$

$$\bar{h}^{02} = A_5 K_0(sVr). \tag{68}$$

where A_4 and A_5 denote the integration parameters.

Using relationship (64) and incorporating Equation (65) into (48), we obtain:

$$\bar{E}^{01} = -\frac{1}{V} A_4 I_1(sVr). \tag{69}$$

$$\bar{E}^{02} = \frac{1}{V} A_5 K_1(sVr). \tag{70}$$

When both sides of Equation (44) are differentiated for r , we obtain:

$$\frac{d\bar{u}}{dr} = \sum_{i=1}^3 \left(A_i \left[I_0(m_i r) - \frac{1}{m_i r} I_1(m_i r) \right] + B_i \left[K_0(m_i r) + \frac{1}{m_i r} K_1(m_i r) \right] \right) \tag{71}$$

When Equations (60), (63), and (71) are substituted into Equation (49), the components of the stress tensor are given as:

$$\begin{aligned} \bar{\sigma}_{rr} = & \sum_{i=1}^3 A_i \left[\left(1 - \frac{q\delta_1^2}{m_i^2 - q} \right) I_0(m_i r) - \frac{(1-c_1)}{m_i r} I_1(m_i r) \right] \\ & + \sum_{i=1}^3 B_i \left[\left(1 - \frac{q\delta_1^2}{m_i^2 - q} \right) K_0(m_i r) + \frac{(1-c_1)}{m_i r} K_1(m_i r) \right], \end{aligned} \tag{72}$$

$$\begin{aligned} \bar{\sigma}_{\xi\xi} = & \sum_{i=1}^3 A_i \left[\left(c_1 - \frac{q\delta_1^2}{m_i^2 - q} \right) I_0(m_i r) + \frac{(1-c_1)}{m_i r} I_1(m_i r) \right] \\ & + \sum_{i=1}^3 B_i \left[\left(c_1 - \frac{q\delta_1^2}{m_i^2 - q} \right) K_0(m_i r) - \frac{(1-c_1)}{m_i r} K_1(m_i r) \right] \end{aligned} \tag{73}$$

$$\begin{aligned} \bar{\sigma}_{zz} = & \sum_{i=1}^3 A_i \left[\left(c_2 - \frac{q\delta_1^2}{m_i^2 - q} \right) I_0(m_i r) - \frac{(c_2-c_1)}{m_i r} I_1(m_i r) \right] \\ & + \sum_{i=1}^3 B_i \left[\left(c_2 - \frac{q\delta_1^2}{m_i^2 - q} \right) K_0(m_i r) + \frac{(c_2-c_1)}{m_i r} K_1(m_i r) \right]. \end{aligned} \tag{74}$$

After substituting Equation (63) into (50), we obtain:

$$\bar{\tau}_{rr} = -\delta_2 m_0 \sum_{i=1}^3 \left(\frac{s}{m_i^2 - \varphi_2} \right) [A_i I_0(m_i r) + B_i K_0(m_i r)]. \tag{75}$$

After applying the Laplace transforms, the boundary conditions (41)–(46) are converted to:

$$\bar{\theta}(r, s) = \frac{\theta_0}{s} \quad \text{at } r = a, \tag{76}$$

$$\frac{d\bar{\theta}(r, s)}{dr} = 0 \quad \text{at } r = b, \tag{77}$$

$$\bar{\sigma}_{rr}(r, s) = 0 \quad \text{at } r = a, \tag{78}$$

$$\bar{\sigma}_{rr}(r, s) = 0 \quad \text{at } r = b, \tag{79}$$

$$\bar{E}(r, s) = \bar{E}^{01}(r, s) \quad \text{at } r = a, \tag{80}$$

$$\bar{h}(r, s) = \bar{h}^{01}(r, s) \quad \text{at } r = a. \tag{81}$$

$$\bar{E}(r, s) = \bar{E}^{02}(r, s) \quad \text{at } r = b, \tag{82}$$

$$\bar{h}(r, s) = \bar{h}^{02}(r, s) \quad \text{at } r = b. \tag{83}$$

Substituting the solution functions into the above boundary conditions (Equations (60), (61), (65), (67)–(70), and (72)) yields a linear system of equations with unknown parameters, A_i , with $i = 1, 2, \dots, 5$, and B_i , with $i = 1, 2, 3$. By solving this system, the values of these constants can be set. As a result, an integrated solution to the problem is achieved in the field of the Laplace transform. Now, we have to find the inverse transformations of the solutions of the studied system domains to the space–time domain.

6. Numerical Inversion of Laplace Transforms

Solving the Laplace transform numerical inversion on the real axis has long been challenging. This is a hot topic in scientific computing, as evidenced by the high number of articles on it that have been published. It is possible to solve this inverse problem in several ways (see, for example, [37–40]). Most numerical techniques include one or more adjusting factors that influence the accuracy and precision of the computation. For an accuracy check, one can utilize these tuning or scaling settings. By performing the same calculations with various tuning or scaling values, it is possible to determine how accurate the result will be since the computation changes with the tuning parameters.

A numerical method for calculating the inverse Laplace transform of actual data is provided in this section. We use a numerical reversal technique for the governing fields based on applying the Fourier series to reverse the Laplace transformation. Dubner and Abate [36] investigated the use of the Fourier series to compute inverse Laplace transformations. One value of t is entered into one of these methods to find the original function, $f(t)$. For a given value of time t and a positive number ζ , the following relationship can be used to find the approximate value of the original $f(r, t)$:

$$f(r, t) = \frac{e^{\zeta t}}{t} \left(\frac{1}{2} \bar{f}(r, \zeta) + \operatorname{Re} \sum_{n=1}^m (-1)^n \bar{f} \left(r, \zeta + \frac{in\pi}{t} \right) \right). \tag{84}$$

According to Durbin [41], the best results were obtained when $\zeta t = 5$ to 10 and m was between 50 and 5000.

7. Graphical Results and Discussion

For computational reasons, a material with physical constants that is transversely isotropic is proposed. We consider a numerical case for which numerical solutions are offered to illustrate the previously supplied analytical approach and contrast the theoretical conclusions from the preceding sections. A numerical computation is created using the Mathematica software package. The physical constants of magnesium (Mg) are listed as follows [31]:

$$\begin{aligned} c_{11} &= 4.96 \times 10^{14} \text{kg m}^{-1} \text{s}^{-2}, \quad c_{12} = 1.15 \times 10^{14} \text{kg m}^{-1} \text{s}^{-2}, \quad \rho = 8954 \text{kg m}^{-3}, \\ \beta_{rr} &= \beta_{\zeta\zeta} = 1.718 \times 10^8 \text{kg m}^{-2} \text{s}^{-2}, \quad C_E = 2 \times 10^2 \text{J/kgK}, \quad T_0 = 298 \text{K}, \quad \theta_0 = 1, \\ \epsilon_0 &= 10^{-9} / (36\pi) \text{Fm}^{-1}, \quad \mu_0 = 10^{-7} \times (4\pi) \text{Hm}^{-1}, \quad H_0 = 10^7 / (4\pi) \text{Am}^{-1}, \\ \sigma_0 &= 10^{-7} \times (4\pi) \Omega^{-1} \text{m}^{-1}, \quad K = 96 \text{W m}^{-1} \text{K}^{-1}, \quad K_0^* = 2 \text{W m}^{-1} \text{K}^{-1} \text{s}^{-1}, \end{aligned}$$

In the calculations, we use the inner radius of the cavity as $a = 1$; the outer radius as $b = 2$, with respect to the center of the hole; and one value of time ($t = 0.12$) unless otherwise specified.

In three scenarios, numerical computations are performed. The first scenario examines how the non-dimensional field variables fluctuate with the magnetic field, while time and relaxation time stay constant. The second objective is to examine how non-dimensional temperature change θ , radial displacement u , and thermal stresses (σ_{rr} and $\sigma_{\zeta\zeta}$) fluctuate for various thermoelastic models while time remains constant. The third instance investigates how the studied non-dimensional fields fluctuate with time while all other parameters are held constant. The numerical results of the fields of study are represented in tables and figures for the purpose of comparison and the discussion of the problem.

7.1. The Effect of the Applied Magnetic Field

Because it can be used in many different fields, including Earth sciences, plasma physics, nuclear engineering, and other similar topics, the mechanical properties and how electromagnetic forces, temperature, pressure, and strain affect each other in a thermoelastic material are very important topics of investigation. The ability of magnetic materials to exhibit reversibility, that is, the production of electric charge in response to an applied mechanical force and the internal generation of mechanical vibration in response to an applied electric field, are among their greatest properties. Due to their intrinsic properties, magnetic materials are widely used in the fields of electrical and electronic engineering, structural engineering, medical equipment, and contemporary industry.

The present section focuses on studying thermoelasticity waves in a hollow, flexible cylinder that conducts electricity and has a stress-free boundary. The cylinder is placed inside a magnetic field surrounding its inner surface. While maintaining constant relaxation time (τ_0) and transit time (t) parameters, the first situation is a study of non-dimensional investigated field variables using the proposed generalized Moore–Gibson–Thompson thermoelasticity (MGTTE) model in the presence $\left(H_0 = \frac{10^7}{4\pi} = H_1 \text{ and } H_0 = \frac{10^8}{4\pi} = H_2 \right)$

and absence of the electromagnetic field effect ($H_0 = 0$). If parameters m_0 , V^2 , and δ_2 , which are defined in equation (36), are all equal to zero, the generalized thermoelasticity equations do not include magneto-electric influences. Changes in the spatial coordinates can be seen in Figures 2–6.

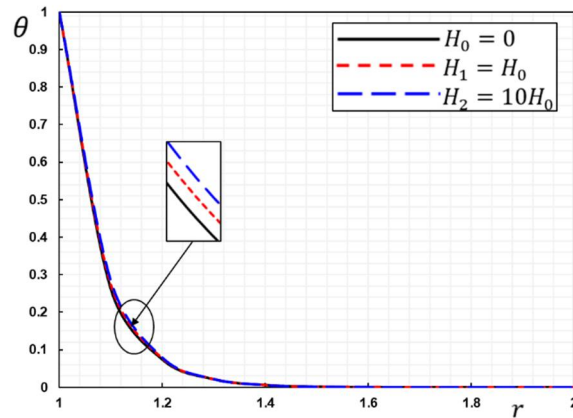


Figure 2. The temperature change, θ , versus the axial magnetic field, H_0 .

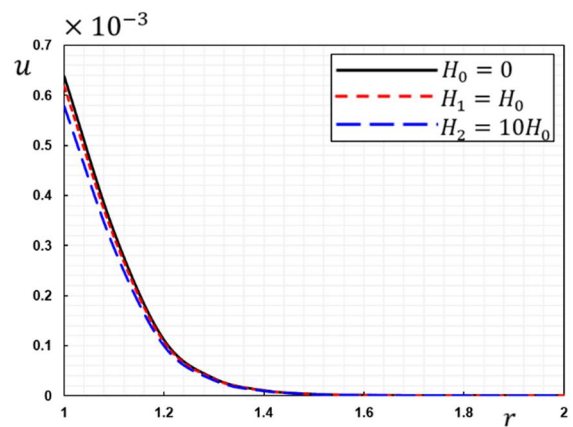


Figure 3. The displacement distribution, u , versus the axial magnetic field, H_0 .

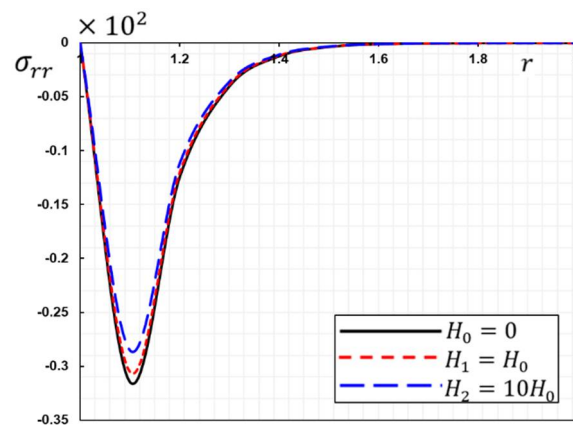


Figure 4. The radial thermal stress, σ_{rr} , versus the axial magnetic field, H_0 .

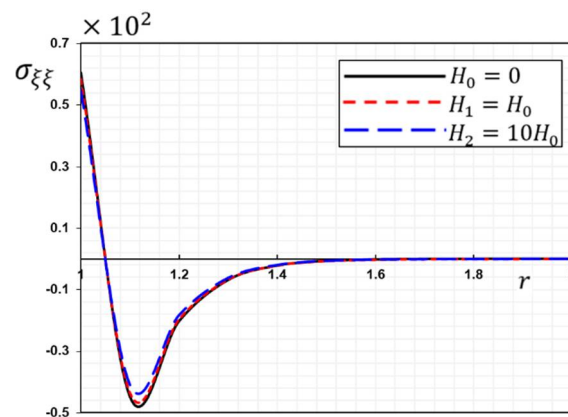


Figure 5. The hoop thermal stress, $\sigma_{\xi\xi}$, versus the axial magnetic field, H_0 .

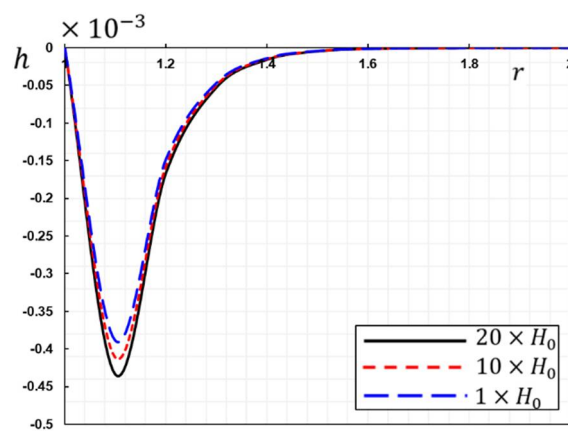


Figure 6. The induced magnetic field, h , versus the axial magnetic field, H_0 .

It is clear from the curves in the figures that the nature of the variation in the fields varies with time. The data clearly show that the applied magnetic field significantly affects each field under investigation. The phenomenon of finite propagation velocity is also found in all figures. On the other hand, the propagation speed in the case of the coupled and uncoupled classical theories of thermoelasticity is infinite; all the functions involved have infinite values at every point in the medium away from sources and thermal shocks.

The variation in temperature c across the radial distance is shown in Figure 2. The temperature changes are initially of larger magnitudes and become smaller over time to ensure that they meet the boundary requirements, as shown in Figure 2. In addition, for all values of H_0 , it goes down quickly as the distance from the center increases and goes away before $r = 1.5$. The heat wave front moves forward over time at a finite pace. The graph shows that only in a finite space field at a given moment, the temperature has a non-zero value. Thermal oscillation is sensed in the region close to the heat shock, and the turbulence disappears outside this region. In many locations, the non-zero region moves all the time, consistently. Although the magnetic field has a slight effect on the temperature distribution, it helps to increase the amount of temperature change.

Figure 3 represents the variation in radial displacement u versus radial distance r for different values of the magnetic field. Figure 3 depicts the displacement variation, starting with positive values in all situations and decreasing to zero over time. This distortion is the result of a dynamic phenomenon. When magnetic field H_0 values increase, we see a decrease in the magnitudes of the displacement. It can be seen from Figure 2 that the wave effect limits the temperature of the non-zero region of the radial displacement at a given moment. Over time, it appears that heat is transmitted to the deeper layers of the medium at a limited rate. The thermal turbulence and the radial displacement area go up directly with the investigated moment.

Figure 4 shows how radial tension σ_{rr} varies with radial position r in each example. It should be noticed that radial stress σ_{rr} rapidly rises to zero values after immediately decreasing from zero to a minimum value. As can be seen in Figure 4, thermal stress σ_{rr} fluctuations at the side walls of the hollow cylinder with $r = 1$ and $r = 2$ correspond to the boundary conditions, as they always start and end with zero values. The values of initial magnetic field H_0 raise pressure σ_{rr} , which is another observation that can be gleaned from the graph. The tension affects the material on the inner surface of the cylinder. This change corresponds to the radial expansion deformation of the medium, as in Figure 3. In addition, it is observed that the compressed region shrinks with time, and the tensile stress region grows, which is consistent with the previously mentioned dynamic stretching effect. Figure 4 also shows that the area of non-zero stress is limited at some point near the heat shock. This shows how temperature waves affect the current change in stress σ_{rr} .

Elastic elements and systems subjected to mechanical loads while immersed in a magnetic field with a large energy variation can experience a wide range of stresses. The generated electrodynamic losses add thermal stress, and the Lorentz force adds magnetic stress to the already present mechanical stress. As well as influencing one another, these stressors are very complicated. Validating the current conclusions requires closely fitting the new data to the prior data [42]. This means that the accuracy of present numerical estimates is quite good.

Figure 5 depicts the behavior of hoop stress $\sigma_{\zeta\zeta}$ as the radial distance changes with and without the effect of initial magnetic field H_0 changing. As the illustration shows, there is circumferential compressive stress for the transversely isotropic material. It is also clear from the figure that the behavior of circumferential stress $\sigma_{\zeta\zeta}$ is the same as that of radial stress σ_{rr} , but the difference is in the starting point, where the hoop stress starts with positive values different from zero. Compression occurs in one section of the cylinder, while tension occurs in another, as shown in Figures 4 and 5. The area close to the inner surface of the cylinder undergoes increasing tensile stress over time as it fades to the other side. From Figure 4, we can find that the amount of stress $\sigma_{\zeta\zeta}$ increases as the magnetic field immersing the cylinder increases. This shows that the effect of parameter H_0 develops further into the hollow cylinder, in addition to the effect of thermal shock.

Figures 6–8 depict non-dimensional induced magnetic field h , induced electric field E , and the radial Maxwell stress τ_{rr} distribution in the hollow cylinder with three different values of axial magnetic field H_0 . The associated thermo-elastic and electromagnetic interactions can be easily found in Figures 6–8. Thermal shock causes the deformation of the electromagnetic medium, which is initially in a magnetic field. As a result, the magnetic flux passing through the cross-section of the cylinder changes. Thus, the medium contains an induced magnetic field in addition to an induced electric field. As the heat wave moves deeper into the cylinder, the magnetic and electric fields that it creates change. This is further proof that heat moves in a waveform.

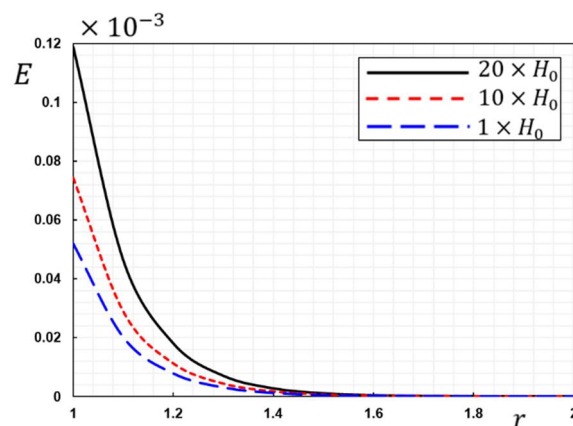


Figure 7. The induced electric field, E , versus the axial magnetic field, H_0 .

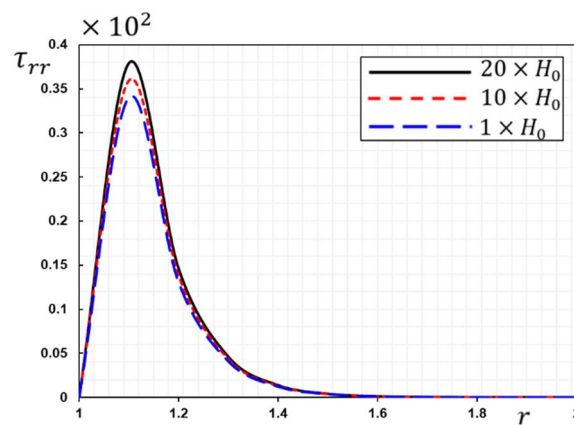


Figure 8. The radial Maxwell stress, τ_{rr} , versus the axial magnetic field, H_0 .

According to the figures and numerical results, the coefficient of variation in axial magnetic field H_0 has a significant effect on the behavior of all induced fields, whether electric or magnetic, which increases the importance of considering the effect of axial magnetic field H_0 . It is clear from looking at Figures 6–8 that when H_0 is equal to $\frac{10^9}{4\pi}$ and $\frac{10^8}{4\pi}$, the absolute values of all the field variables are higher than they are when H_0 is equal to $\frac{10^7}{4\pi}$.

Thermo-magneto-elastic investigations of plates and shells have previously heavily relied on linear models and simplified ideas. In reality, however, most plate and shell constructions are subjected to high-energy, temperature-varying electromagnetic radiations, resulting in strongly coupled deformations [43]. Sheets and circular panels are used in engineering for things such as pneumatics, turbine diaphragms, marine structures, nuclear reactors, optical systems, shipbuilding, cars and other vehicles, space shuttles, sound emitters and receivers, ports and swivel panels, and other annular tapers [44].

7.2. Comparison of Different Models of Thermoelasticity

In the second scenario of this discussion, the behavior of non-dimensional thermal and mechanical field variables as well as electromagnetic variables versus radial distance r are explored in the case of various thermoelastic theories. In this case, axial magnetic field H_0 and time t remain the same. Figures 8–14 depict a different variant of the physical fields each to illustrate the differences between the different theories of thermoelasticity and their relationship to each other. The model proposed in this article presents many previous models in the general thermoelastic theory as special cases. The coupled dynamical thermoelasticity theory (CTE) can be obtained when $\tau_0 = K^* = 0$, while the Lord–Shulman model (LS) is in the case of $K^* = 0$. In addition, the second type of the Green–Naghdi theorem (GN-II) can be derived when the term that includes parameter K is equal to zero and there is no thermal relaxation time. On the other hand, when neglecting the thermal relaxation time, the third type (GN-III) can be produced. In the presence of thermal relaxation τ_0 , and K^* and K parameters, we have the Moore–Gibson–Thompson generalized thermoelastic theory (MGTTE).

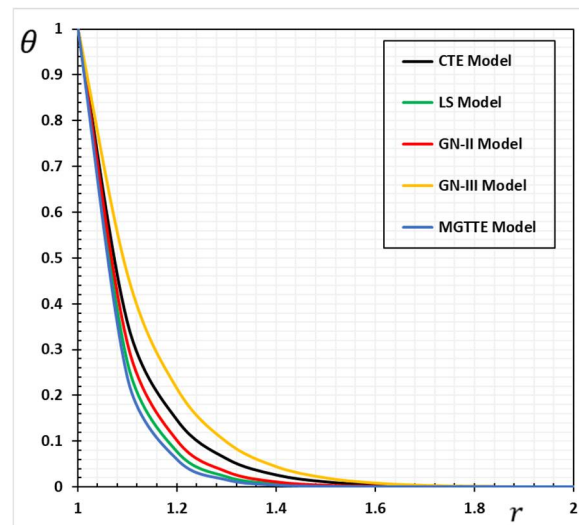


Figure 9. The temperature change, θ , versus different thermoelastic models.

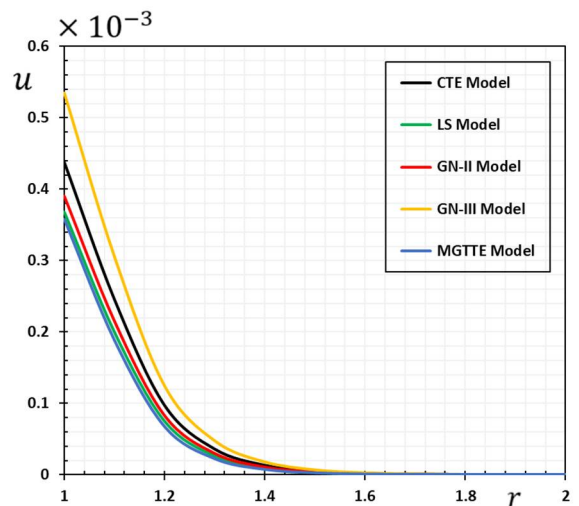


Figure 10. The displacement, u , versus different thermoelastic models.

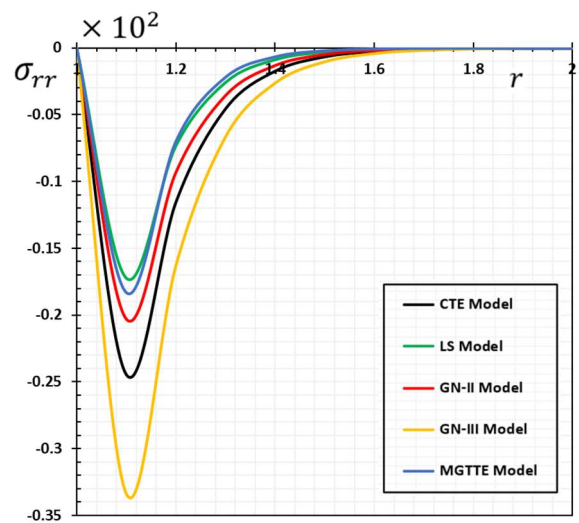


Figure 11. The radial stress, σ_{rr} , versus different thermoelastic models.

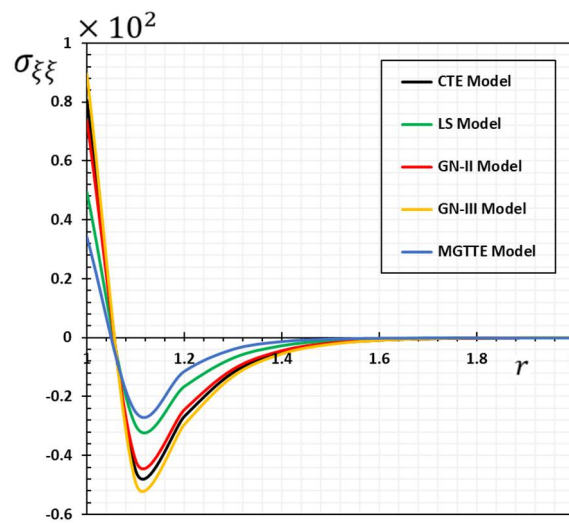


Figure 12. The hoop stress, $\sigma_{\xi\xi}$, versus different thermoelastic models.

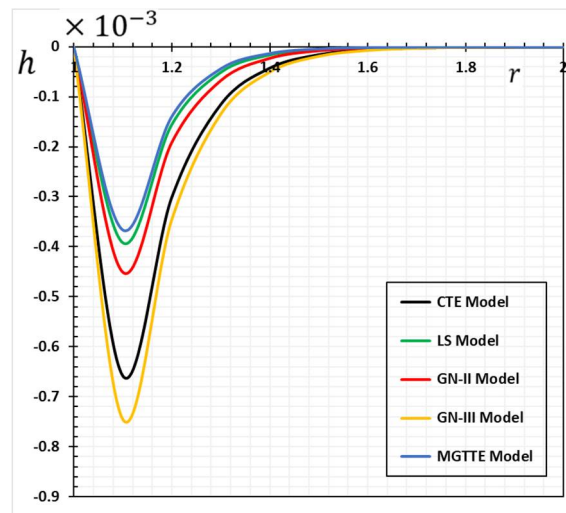


Figure 13. The induced magnetic field, h , versus different thermoelastic models.

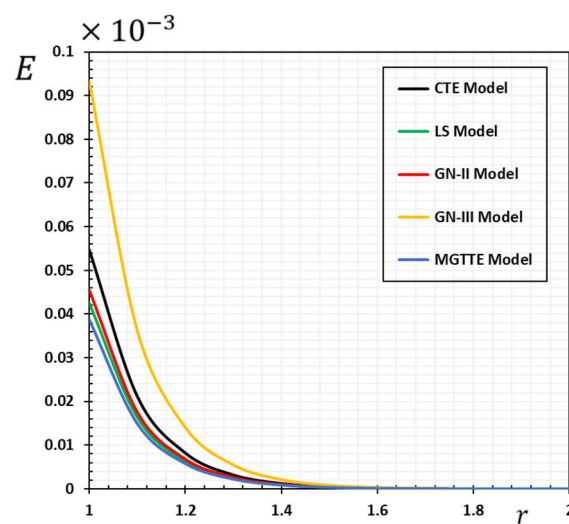


Figure 14. The induced electric field, E , versus different thermoelastic models.

This subsection presents the results in Tables 1–7 and Figures 9–15, aiming to facilitate comparisons between different thermoelastic models. Future scientists can compare their results using the tables in this article. Looking at the tables and noting Figures 5–8, it can be seen that the thermal parameters strongly influence the distribution of the studied field quantities, τ_0 and K^* . It is also evident that the values of the fields vary with different thermal models. Both the generalized (LS, GNII, GNIII, and MGTTE) and coupled (CTE) thermoelastic models provide remarkably similar results in behavior near the inner cylinder surface where the boundary conditions imposed by the proposed problem are present. The findings, which are consistent with generalized thermoelasticity theories, are extremely comparable as the distance rises.

Table 1. The temperature, θ , versus different models of thermoelasticity.

r	CTE	LS	GN-II	GN-III	MGTTE
1	1.002670000	1.002670000	1.002670000	1.002670000	1.002670000
1.1	0.359209000	0.271741000	0.313294000	0.464869000	0.238439000
1.2	0.146344000	0.076977000	0.101408000	0.215363000	0.059891700
1.3	0.061846600	0.022179500	0.033254400	0.098890400	0.015379900
1.4	0.026386200	0.006437660	0.010968100	0.045027300	0.003987100
1.5	0.011284000	0.001875910	0.003629730	0.020348100	0.001038560
1.6	0.004829320	0.000548098	0.001204270	0.009143340	0.000271333
1.7	0.002071650	0.000160556	0.000400793	0.004117240	7.106×10^{-5}
1.8	0.000901008	4.739×10^{-5}	0.000134906	0.001920390	1.87×10^{-5}
1.9	0.000424842	1.4958×10^{-5}	0.000049294	0.001038900	5.13×10^{-6}
2	0.000295683	8.04×10^{-6}	2.954×10^{-5}	0.000809694	1.75×10^{-6}

Table 2. The displacement, u , versus different models of thermoelasticity.

r	CTE	LS	GN-II	GN-III	MGTTE
1	0.437701000	0.368473000	0.390555000	0.534831000	0.357523000
1.1	0.245658000	0.200020000	0.215465000	0.305815000	0.188293000
1.2	0.097118700	0.075013900	0.082896900	0.124531000	0.067335300
1.3	0.035868700	0.026147200	0.029716500	0.047508500	0.022276600
1.4	0.013041300	0.008954700	0.010476400	0.017861300	0.007227640
1.5	0.004729020	0.003056390	0.003682310	0.006699820	0.002335400
1.6	0.001715730	0.001043540	0.001294830	0.002514630	0.000754696
1.7	0.000622736	0.000356514	0.000455545	0.000944092	0.000244065
1.8	0.000226819	0.000122126	0.000160750	0.000355996	7.911×10^{-5}
1.9	9.70×10^{-5}	4.79×10^{-5}	6.57×10^{-5}	0.000160252	2.88×10^{-5}
2	9.94×10^{-5}	4.45×10^{-5}	6.41×10^{-5}	0.000172770	2.45×10^{-5}

Table 3. The radial stress, σ_{rr} , versus different models of thermoelasticity.

r	CTE	LS	GN-II	GN-III	MGTE
1.0	0	0	0	0	0
1.1	−0.244336000	−0.172155000	−0.202867000	−0.333905000	−0.183058000
1.2	−0.115397000	−0.073163500	−0.093051000	−0.163042000	−0.069810200
1.3	−0.045451000	−0.025694200	−0.035503100	−0.066585000	−0.021800700
1.4	−0.017213800	−0.008634780	−0.013008300	−0.026186200	−0.006481430
1.5	−0.006464920	−0.002871200	−0.004723640	−0.010218800	−0.001901870
1.6	−0.002426830	−0.000953299	−0.001713980	−0.003986920	−0.000556607
1.7	−0.000912297	−0.000316861	−0.000622786	−0.001557630	−0.000162984
1.8	−0.000336369	−0.000104393	−0.000222791	−0.000593694	$−4.75 \times 10^{-5}$
1.9	$−6.98 \times 10^{-5}$	$−2.51 \times 10^{-5}$	$−4.91 \times 10^{-5}$	−0.000112554	$−1.15 \times 10^{-5}$
2.0	0	0	0	0	0

Table 4. The hoop stress, $\sigma_{\zeta\zeta}$, versus different models of thermoelasticity.

r	CTE	LS	GN-II	GN-III	MGTE
1	−0.1674230	−0.16390100	−0.16847300	−0.1679220	−0.16461300
1.1	−0.1056410	−0.11924100	−0.12504200	−0.1243420	−0.14136000
1.2	−0.2389110	−0.34152100	−0.35182600	−0.2699060	−0.42123700
1.3	−0.1761530	−0.00034987	−0.35506100	−0.2113800	−0.00087196
1.4	−0.1299800	−0.00559739	−0.00043307	−0.1648920	−0.00736980
1.5	−0.0923387	−0.00434826	−0.00162313	−0.1252300	−0.00670395
1.6	−0.0660684	−0.00353167	−0.00186000	−0.0974572	−0.00645638
1.7	−0.0497601	$−3.12 \times 10^{-5}$	−0.00189921	−0.0816976	$−2.52 \times 10^{-5}$
1.8	−0.0417722	$−5.74 \times 10^{-5}$	−0.0018784100	−0.0768195	−0.00010373
1.9	−0.0399789	−0.00012725	−0.00181465	−0.0792553	−0.00037063
2	−0.0187146	$−3.95 \times 10^{-5}$	$−4.0 \times 10^{-5}$	−0.0393544	−0.00011718

Table 5. The induced magnetic field, h , versus different models of thermoelasticity.

r	CTE	LS	GN-II	GN-III	MGTE
1	1.04363×10^{-7}	4.83×10^{-8}	7.05×10^{-8}	1.56538×10^{-7}	3.35×10^{-8}
1.1	−0.657885000	−0.39161200	−0.449990000	−0.744555000	−0.36674300
1.2	−0.302240000	−0.15586500	−0.191522000	−0.346977000	−0.14004700
1.3	−0.115489000	−0.05096750	−0.067352000	−0.134657000	−0.04378810
1.4	−0.042371400	−0.01589600	−0.022662100	−0.050209600	−0.01303270
1.5	−0.015404400	−0.00489736	−0.007543730	−0.018556800	−0.00382798
1.6	−0.005595750	−0.00150538	−0.002507180	−0.006853680	−0.00112129
1.7	−0.002037820	−0.00046323	−0.000834675	−0.002538090	−0.000328693
1.8	−0.000748352	−0.00014319	−0.000279609	−0.000948138	$−9.67082 \times 10^{-5}$
1.9	−0.000269318	$−4.3415 \times 10^{-5}$	$−9.19098 \times 10^{-5}$	−0.000346829	$−2.78989 \times 10^{-5}$
2	7.16×10^{-8}	7.2×10^{-6}	2.34×10^{-8}	5.49×10^{-8}	5.74×10^{-10}

Table 6. The induced electric field, E , versus different models of thermoelasticity.

r	CTE	LS	GN-II	GN-III	MGTE
1	0.054825500	0.042532900	0.045444800	0.093388400	0.038801500
1.1	0.021246700	0.016445700	0.017583000	0.036310200	0.014988600
1.2	0.008245870	0.006369620	0.006814010	0.014134000	0.005800250
1.3	0.003206120	0.002472400	0.002646170	0.005509270	0.002249780
1.4	0.001249660	0.000962532	0.001030530	0.002151130	0.000875425
1.5	0.000488775	0.000376317	0.000402948	0.000841861	0.000342202
1.6	0.000192136	0.000148042	0.000158484	0.000330547	0.000134663
1.7	7.60912×10^{-5}	5.87733×10^{-5}	0.000062876	0.000130407	5.35157×10^{-5}
1.8	3.04678×10^{-5}	2.36483×10^{-5}	0.000025265	5.18156×10^{-5}	2.15752×10^{-5}
1.9	0.000012398	9.7000×10^{-6}	1.03412×10^{-5}	2.08084×10^{-5}	8.8800×10^{-6}
2	5.1600×10^{-6}	4.0900×10^{-6}	4.3400×10^{-6}	8.4900×10^{-6}	3.7600×10^{-6}

Table 7. The radial Maxwell stress, τ_{rr} , versus different models of thermoelasticity.

r	CTE	LS	GN-II	GN-III	MGTE
1	3.16×10^{-6}	6.09×10^{-6}	7.34×10^{-6}	9.49×10^{-6}	6.44×10^{-6}
1.1	0.255101000	0.221500000	0.237873000	0.273060000	0.206062000
1.2	0.085469500	0.069369300	0.077010800	0.094794400	0.062490100
1.3	0.023206900	0.017518800	0.020153600	0.026741800	0.015246600
1.4	0.005961050	0.004172220	0.004981440	0.007148730	0.003502770
1.5	0.001506170	0.000975682	0.001210080	0.001881510	0.000789508
1.6	0.000378929	0.000226982	0.000292558	0.000493300	0.000176949
1.7	9.53214×10^{-5}	5.27723×10^{-5}	7.07047×10^{-5}	0.000129354	3.96246×10^{-5}
1.8	2.41088×10^{-5}	1.23214×10^{-5}	1.71696×10^{-5}	3.41292×10^{-5}	8.91×10^{-6}
1.9	6.9×10^{-5}	3.24×10^{-6}	4.7×10^{-6}	1.02397×10^{-5}	2.25×10^{-6}
2	1.04363×10^{-5}	4.83×10^{-6}	7.05×10^{-6}	1.56538×10^{-5}	3.35×10^{-6}

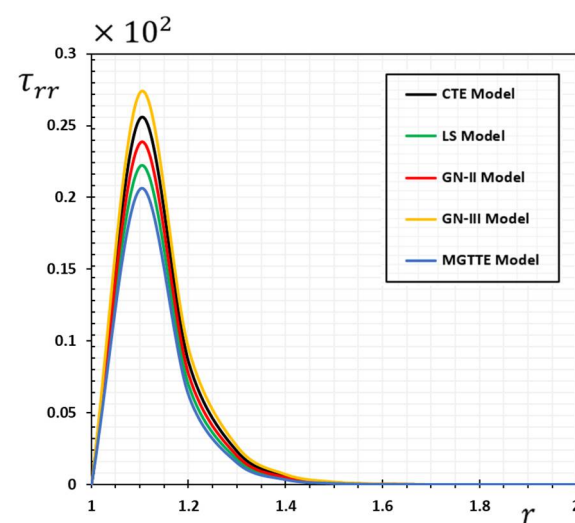


Figure 15. The radial Maxwell stress, τ_{rr} , versus different thermoelastic models.

In contrast with generalized thermoelastic models, which assume that heat waves move at a limited speed, the coupled theory says that heat waves move at an unlimited speed. The numerical results show that the heat wave travels from the inside of the cylinder to the outside because the thermal shock is applied only to the inner surface of the cylinder.

Tables 1–4 and Figures 9–15 show the discrepancy between the predictions of the GN-III model and the MGTE model. The results show that the numerical values and curves in the case of the GN-III model are greater than the values and fields of the curves in the case of the MGTE model. It is noticed that the numerical values of both the LS and MGTE models show similar results and behaviors. The reason for this is that there is a thermal relaxation time. The results of the Green and Naghdi type III thermoelastic model (GN-III) show that they differ significantly from the small energy dissipation type II thermoelastic concepts (GN-II) [16,27]. When comparing the GN-II model with other models, it can be seen that the temperature values and distributions are very different.

These illustrations clearly show that the waves propagate at limited rates in the extended Moore–Gibson–Thompson thermoelasticity theory (MGTTE). We see that all variables disappear uniformly outside a time-varying, finite region. This is not true for coupled thermoelasticity (CTE) and Green and Naghdi type III, where the function under consideration has non-vanishing values for all values of r because heat waves spread at an unlimited rate. Compared with previous generalized models of thermoelasticity, the results of GN-III show convergence with the classical elasticity model (CTE) results, which do not fade quickly under the influence of heat inside the medium. This matches perfectly with the information provided by Quintanilla [25], which is why the new model is proposed in this article.

8. Conclusions

The main objective of the present work is to investigate the effects of a detailed analysis of thermally induced and mechanical vibrations of a transverse, thermoelastic, long, hollow cylinder under the proposed Moore–Gibson–Thompson (MGTTE) thermoelastic model. The governing equations of the system are solved using the Laplace transform method to figure out the studied physical fields.

According to the results of the study, the most important conclusions can be summarized as follows:

- The applied axial magnetic field significantly influences the increase or decrease in the researched field variables through the thermoelastic materials in the investigated fields. Nevertheless, it has a small influence on the non-dimensional temperature;
- When electromagnetic radiation hits flexible structures, it creates different temperature differences and a lot of energy, which distorts the highly coupled medium;
- In the expanded Moore–Gibson–Thompson thermoelastic model, thermal waves are dispersed as finite-velocity waves rather than infinite waves in a transversely isotropic material, as in the conventional thermoelastic theory. In addition, there was convergence and similarity between the GN-III and CTE models, which indicates the validity and relevance of the presented thermoelastic model;
- Both the LS and MGTE models show similar results and similar behaviors. The reason for this is that there is a thermal relaxation time.

Finally, the methodology described in this article applies to many thermodynamic challenges. The diaphragms of turbines, aircraft and missiles, marine structures, nuclear reactors, optical systems, shipbuilding, automobiles and other vehicles, space shuttles, sound emitters and receivers, ports and rotating plates, and other annular structures are just a few of the engineering applications of these circular sheets and plates. Experimental scientists and researchers who study this field can also benefit from these theoretical findings.

Author Contributions: Conceptualization, O.M. and A.E.A.; methodology, A.E.A. and F.A.; software, O.M.; formal analysis, O.M.; investigation, A.E.A. and F.A.; writing—original draft preparation, F.A.; writing—review and editing, O.M. and F.A.; project administration, A.E.A. All authors have read and agreed to the published version of the manuscript.

Funding: Deputyship for Research and Innovation, Ministry of Education, Saudi Arabia, funded this research work through the project number QU-IF-2-5-3-27713.

Data Availability Statement: Not applicable.

Acknowledgments: The authors extend their appreciation to the Deputyship for Research & Innovation, Ministry of Education, Saudi Arabia for funding this research work through the project number (QU-IF-05-03-27713). The authors also thank to Qassim University for technical support.

Conflicts of Interest: The authors declare no potential conflicts of interest concerning the research work, authorship, and publication of this article.

Nomenclature

\vec{q} = heat flux vector; K = thermal conductivity; $\theta = T - T_0$ temperature change; T = absolute temperature; T_0 = reference temperature; τ_0 = relaxation time; \vec{x} = position vector; K^* = thermal conductivity rate; ϑ = thermal displacement; C_E = specific heat; Q = heat source; ρ = material density; t = time variable; $\beta_{ij} = c_{ijkl}\alpha_{kl}$, coefficients of thermal coupling; α_{kl} , coefficients of linear thermal expansion; c_{ijkl} = elastic constants; σ_{ij} = stress tensor; e_{ij} = strain tensor; u_i = the components of the displacement vector. In addition, \vec{J} = electric current density; \vec{E} = induced electric field vector; \vec{h} = induced magnetic field vector; \vec{B} = magnetic induction vector; \vec{D} = electric induction vector; μ_0 = magnetic permeability; ϵ_0 = electric permeability; F_i , components of body force; σ_0 = electric conductivity.

References

1. Biot, M.A. Thermoelasticity and irreversible thermodynamics. *J. Appl. Phys.* **1956**, *27*, 240–253. [\[CrossRef\]](#)
2. Cattaneo, C. A form of heat-conduction equations which eliminates the paradox of instantaneous propagation. *Compt. Rend.* **1958**, *247*, 431–433.
3. Lord, H.W.; Shulman, Y. A generalized dynamical theory of thermoelasticity. *J. Mech. Phys. Solids* **1967**, *15*, 299–309. [\[CrossRef\]](#)
4. Green, A.E.; Lindsay, K.A. Thermoelasticity. *J. Elast.* **1972**, *2*, 1–7. [\[CrossRef\]](#)
5. Green, A.E.; Naghdi, P.M. A re-examination of the basic postulates of thermomechanics. *Proc. R. Soc. Lond.* **1991**, *432*, 171–194.
6. Green, A.E.; Naghdi, P.M. On undamped heat waves in an elastic solid. *J. Therm. Stress.* **1992**, *15*, 253–264. [\[CrossRef\]](#)
7. Green, A.E.; Naghdi, P.M. Thermoelasticity without energy dissipation. *J. Elast.* **1993**, *31*, 189–209. [\[CrossRef\]](#)
8. Abouelregal, A.E.; Civalek, Ö.; Öztop, H.F. Higher-order time-differential heat transfer model with three-phase lag including memory-dependent derivatives. *Inter. Commun. Heat Mass Trans.* **2021**, *128*, 105649. [\[CrossRef\]](#)
9. Abouelregal, A.E.; Marin, M.; Alsharari, F. Thermoelastic plane waves in materials with a microstructure based on micropolar thermoelasticity with two temperature and higher order time derivatives. *Mathematics* **2022**, *10*, 1552. [\[CrossRef\]](#)
10. Abouelregal, A.E. An advanced model of thermoelasticity with higher-order memory-dependent derivatives and dual time-delay factors. *Waves Random Complex Media* **2020**, 1–22. [\[CrossRef\]](#)
11. Abouelregal, A.E. A novel model of nonlocal thermoelasticity with time derivatives of higher order. *Math. Methods Appl. Sci.* **2020**, *43*, 6746–6760. [\[CrossRef\]](#)
12. Abouelregal, A.E. Generalized mathematical novel model of thermoelastic diffusion with four phase lags and higher-order time derivative. *T. Eur. Phys. J. Plus* **2020**, *135*, 263. [\[CrossRef\]](#)
13. Zakaria, K.; Sirwah, M.A.; Abouelregal, A.E.; Rashid, A.F. Photo-thermoelastic model with time-fractional of higher order and phase lags for a semiconductor rotating material. *Silicon* **2021**, *13*, 573–585. [\[CrossRef\]](#)
14. Abouelregal, A.E.; Moustapha, M.V.; Nofal, T.A.; Rashid, S.; Ahmad, H. Generalized thermoelasticity based on higher-order memory-dependent derivative with time delay. *Result Phys.* **2021**, *20*, 103705. [\[CrossRef\]](#)
15. Quintanilla, R. Moore-Gibson-Thompson thermoelasticity. *Math. Mech. Solids* **2019**, *24*, 4020–4031. [\[CrossRef\]](#)
16. Quintanilla, R. Moore-Gibson-Thompson thermoelasticity with two temperatures. *Appl. Eng. Sci.* **2020**, *1*, 100006. [\[CrossRef\]](#)
17. Fernández, J.R.; Quintanilla, R. Moore-Gibson-Thompson theory for thermoelastic dielectrics. *Appl. Math. Mech.-Engl. Ed.* **2021**, *42*, 309–316. [\[CrossRef\]](#)
18. Pellicer, M.; Quintanilla, R. On uniqueness and instability for some thermomechanical problems involving the Moore-Gibson-Thompson equation. *J. Appl. Math. Phys.* **2020**, *71*, 84. [\[CrossRef\]](#)

19. Conti, M.; Pata, V.; Pellicer, M.; Quintanilla, R. On the analyticity of the MGT-viscoelastic plate with heat conduction. *J. Differ. Equ.* **2020**, *269*, 7862–7880. [[CrossRef](#)]
20. Bazarra, N.; Fernández, J.R.; Quintanilla, R. Analysis of a Moore-Gibson-Thompson thermoelastic problem. *J. Comput. Appl. Math.* **2020**, *382*, 113058. [[CrossRef](#)]
21. Kumar, H.; Mukhopadhyay, S. Thermoelastic damping analysis in microbeam resonators based on Moore-Gibson-Thompson generalized thermoelasticity theory. *Acta Mech.* **2020**, *231*, 3003–3015. [[CrossRef](#)]
22. Florea, O.A.; Bobe, A. Moore–Gibson–Thompson thermoelasticity in the context of double porous materials. *Contin. Mech. Thermodyn.* **2021**, *33*, 2243–2252. [[CrossRef](#)]
23. Abouelregal, A.E.; Alesemi, M. Fractional Moore-Gibson-Thompson heat transfer model with nonlocal and nonsingular kernels of a rotating viscoelastic annular cylinder with changeable thermal properties. *PLoS ONE* **2022**, *17*, e0269862. [[CrossRef](#)] [[PubMed](#)]
24. Abouelregal, A.E.; Sedighi, H.M. The effect of variable properties and rotation in a visco-thermoelastic orthotropic annular cylinder under the Moore–Gibson–Thompson heat conduction model. *Proc. Inst. Mech. Eng. Part L J. Mater. Des. Appl.* **2021**, *235*, 1004–1020. [[CrossRef](#)]
25. Abouelregal, A.E.; Sedighi, H.M.; Sofiyev, A.H. Modeling photoexcited carrier interactions in a solid sphere of a semiconductor material based on the photothermal Moore–Gibson–Thompson model. *Appl. Phys.* **2021**, *127*, 845. [[CrossRef](#)]
26. Abouelregal, A.E.; Ahmad, H.; Badr, S.K.; Almutairi, B.; Almohsen, B. Viscoelastic stressed microbeam analysis based on Moore–Gibson–Thompson heat equation and laser excitation resting on Winkler foundation. *J. Low Freq. Noise Vib. Act. Control* **2022**, *41*, 118–139. [[CrossRef](#)]
27. Sheikholeslami, M.; Ebrahimpour, Z. Thermal improvement of linear Fresnel solar system utilizing Al₂O₃-water nanofluid and multi-way twisted tape. *Inter. J. Therm. Sci.* **2022**, *176*, 107505. [[CrossRef](#)]
28. Singh, P.L.; Sarviya, R.M.; Bhagoria, J.L. Thermal performance of linear Fresnel reflecting solar concentrator with trapezoidal cavity absorbers. *Appl. Energy* **2010**, *87*, 541–550. [[CrossRef](#)]
29. Sheikholeslami, M. Numerical investigation of solar system equipped with innovative turbulator and hybrid nanofluid. *Sol. Energy Mater. Sol. Cells* **2022**, *243*, 111786. [[CrossRef](#)]
30. Sheikholeslami, M. Analyzing melting process of paraffin through the heat storage with honeycomb configuration utilizing nanoparticles. *J. Energy Storage* **2022**, *52*, 104954. [[CrossRef](#)]
31. Das, P.; Kar, A.; Kanoria, M. Analysis of magneto-thermoelastic response in a transversely isotropic hollow cylinder under thermal shock with three-phase-lag effect. *J. Therm. Stress.* **2013**, *36*, 239–258. [[CrossRef](#)]
32. He, T.; Cao, L. A problem of generalized magneto-thermoelastic thin slim strip subjected to a moving heat source. *Math. Comput. Model.* **2009**, *49*, 1710–1720. [[CrossRef](#)]
33. Sherief, H.H.; Helmy, K.A. A two-dimensional problem for a half-space in magneto-thermoelasticity with thermal relaxation. *Inter. J. Eng. Sci.* **2002**, *40*, 587–604. [[CrossRef](#)]
34. Nowinski, J.L. *Theory of Thermoelasticity with Applications*; Sijthoff & Noordhoff International Publishers: Alphen aan den Rijn, The Netherlands, 1978.
35. Vernotte, P. Some possible complications in the phenomena of thermal conduction. *Compt. Rend.* **1961**, *252*, 2190–2191.
36. Nowacki, W. *Dynamic Problem of Thermoelasticity*; Noordhoff International: Groningen, The Netherlands, 1975; p. 399.
37. Cohen, A.M. *Numerical Methods for Laplace Transform Inversion*; Springer: New York, NY, USA, 2007.
38. Bellman, R.E.; Kalaba, R.; Lockett, J. *Numerical Inversion of the Laplace Transform*; Elsevier: New York, NY, USA, 1966.
39. Crump, K.S. Numerical inversion of Laplace transforms using a Fourier series approximation. *J. Assoc. Comput. Mach.* **1976**, *23*, 89–96. [[CrossRef](#)]
40. Dubner, H.; Abate, J. Numerical inversion of Laplace transforms by relating them to the finite Fourier cosine transform. *J. Assoc. Comput. Mach.* **1968**, *15*, 115–123. [[CrossRef](#)]
41. Durbin, F. Numerical inversion of Laplace transforms: An efficient improvement to Dubner and Abate’s method. *Comput. J.* **1974**, *17*, 371–376. [[CrossRef](#)]
42. Cen, S.; Xu, J. Analysis of thermo-magneto-elastic nonlinear dynamic response of shallow conical shells. *Engineering* **2018**, *10*, 837–850. [[CrossRef](#)]
43. Tanigawa, Y.; Higuchi, M.; Kawamura, R. Dynamic and quasi-static behaviors of magneto-thermo-elastic stresses in a conducting hollow circular cylinder subjected to an arbitrary variation of magnetic field. *Inter. J. Mech. Sci.* **2008**, *50*, 365–379.
44. Lang, Z.; Li, X. Buckling and vibration analysis of functionally graded magneto-electro-thermo-elastic circular cylindrical shells. *Appl. Math. Model.* **2013**, *37*, 2279–2292. [[CrossRef](#)]